# The H(e,e'n)X Reaction and the Pion Structure Function

J. Arrington, F. Dohrmann, D. F. Geesaman, K. Hafidi,
R. J. Holt(Spokesperson), H. E. Jackson, D. Potterveld,
P. E. Reimer(Spokesperson), C. D. Roberts, E. C. Schulte
K. Wijesooriya(Spokesperson)
*Argonne National Laboratory, Argonne, IL 60439*

C. Keppel
*Hampton University and Jefferson Lab*

R. Ent, N. Liyanage, D. J. Mack
*Jefferson Lab, Newport News, VA 23606*

H. Gao, D. Dutta, H. Xiang, F. Xiong, W. Xue, L. Zue
*Massachusetts Institute of Technology, Cambridge, MA 02139*

D. Gaskell, E. Kinney
*University of Colorado, Boulder, CO 80309*

May 25, 2001

**Abstract**

We propose to measure the semi-inclusive cross section for the H(e,e'n)X reaction for $Q^2 > 1GeV^2$ as a function of x and the outgoing neutron momentum. The leading-neutron proton structure function will be extracted from this measurement. The kinematics are chosen to enhance deep inelastic scattering from the virtual pion cloud in the proton. Scattered electrons will be detected in the HRS and Bigbite spectrometers in Hall A, while the neutrons will be detected in an array of plastic scintillators placed behind the Bigbite spectrometer.

Recent HERA data for the pion structure function in the sea region indicate the surprising result that the sea in the pion is only 1/3 of the sea in the proton. Pionic Drell-Yan data exist in the valence region, while no comparable electron scattering data exist in this region. The proposed study will provide an important check on the method used at HERA to measure the pion structure function by providing data for electron scattering in the valence region which can be compared directly with pionic Drell-Yan data for the pion structure function. The pionic Drell-Yan results at very high x appear to be anomalous. The proposed experiment will also provide a means to check the Drell-Yan results at very high x. Such results provide a window into the quark sub-structure of the Goldstone bosons of QCD and a test of contemporary theory and phenomenology.

# 1 Introduction

Understanding the mesonic and baryonic content of the nucleon is an important issue in nuclear physics. For example, the flavor asymmetry of proton sea has been explained in terms of the mesonic content of the proton. The H(e,e'n)X reaction is excellent for this purpose since one can enhance the sensitivity to the pion content. This reaction should provide benchmark data for a test of nucleon models. In addition, if pion cloud model is reasonable, one could use it to extract the pion structure function from these data.

An important question is whether the structure function of a pion is similar to that for a nucleon. The pseudoscalar mesons are the Goldstone bosons which arise from dynamical chiral symmetry breaking[2]. Because the pion is much lighter than the nucleon or even a constituent quark, one might expect the sea of the pion to be much different from that of the nucleon. The pion, being the lightest meson, is particularly interesting because of its importance in chiral perturbation theory, the meson cloud model[3], providing an explanation of the quark sea in the nucleon[1], and the nuclear force in nuclei[4].

Measurements of the pion structure function at very low x at HERA and very high x at Fermilab seem to be anomalous. The HERA data relied upon deep inelastic electron scattering from a virtual pion in the proton, while the FNAL data employed a pionic Drell-Yan process. The Drell-Yan data extend from Bjorken $x_\pi$ of 0.2 to 0.99, and cover the valence region in the pion. The HERA data rely on the H(e,e'n)X reaction and cover the $x_\pi$ region from $3 \times 10^{-4}$ to 0.01.

The purpose of the present work is to measure semi-inclusive deep inelastic scattering for the reaction H(e,e'n)X in a kinematic regime which overlaps the Drell-Yan data in the moderate x region, say $x_\pi = 0.5$ where the Drell-Yan data are most reliable, and extend the measurements up to an $x_\pi$ of 0.8. Thus, the present experiment will be a check of the virtual pion technique, the technique used by HERA, as well as a check of the high-x Drell-Yan data.

# 2 Scientific Motivation

Recent measurements [5] of the cross section for H(e,e′n)X at HERA indicate that the pion exchange mechanism (see figure 1) contributes significantly to the leading neutrons with low $P_T$. In addition, attempts were made to extract the pion structure function from these data. The results of this work show two interesting findings (see figure 2): (1) the sea in the pion has the same shape in $x$ as the sea in the proton, and (2) the pion sea has approximately one-third of the magnitude as the sea in the proton. This latter result is especially surprising since one expects the pion sea to be two-thirds the value of the proton sea. The value of 2/3 follows from the idea that the sea arises from gluon or pion emission from the valence quarks and antiquarks. The data are even more surprising from the viewpoint of a chiral quark model[6]. This model predicts that the pion sea carries a larger momentum fraction than the proton sea. Since the conclusions from HERA rely on the Sullivan mechanism in order to extract the pion structure function, it is essential to check the validity of the Sullivan mechanism as a means of measuring the pion structure function.

Another very interesting puzzle occurs at high x in the pion. In the valence region pionic Drell-Yan data exist[7], and the u quark distribution in the $\pi^-$ has been measured as shown in Fig. 3. Several theoretical calculations are aimed at explaining the pion structure function in the valence region. These include Dyson-Schwinger[9], Nambu Jona-Lasinio[10, 11], and a light-front constituent quark models[13]. Lower order moments of the structure function were determined in lattice gauge calculations[12]. The general features of the valence structure of the pion are qualitatively understood. However, there are some puzzling disagreements at high x. The first puzzle is that the data are in disagreement with the pQCD predictions. According to pQCD, the high x structure function and elastic form factor should be related by the

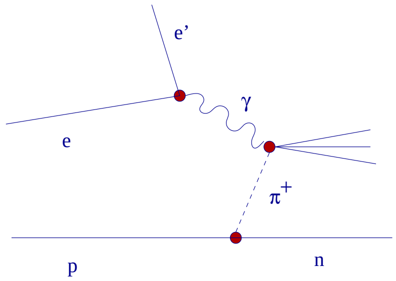


Figure 1: The Sullivan process: Deep inelastic scattering from the pion cloud surrounding a proton.

number of constituent quarks and the spin of the hadron. This would imply that the pion structure function[15] should go as $(1-x)^2$. However, the data resemble a $(1-x)$ dependence. The second puzzle is that the Schwinger-Dyson calculations disagree with the data at high x as shown in Fig. 3. That discrepancy is also observed in other covariant calculations[15][14]. A possible problem with Drell-Yan data at high x is that there appears to be significant longitudinal photon polarization suggesting that the simple Drell-Yan mechanism is breaking down. In addition, although a $\pi^-$ beam was used for these measurements, a W target was used. It is possible that nuclear effects provide problems in extracting the results at very high x. It is essential to check these Drell-Yan data for the pion in the high x region. Confirmation of the $(1-x)$ dependence would provide a serious challenge of our understanding of QCD's Goldstone boson.

The importance of the present proposal is that we will provide semi-inclusive structure functions for the H(e,e$'$n)X reaction in an interesting kinematic regime. In addition, the data will offer a means to check the validity of the Sullivan mechanism in the moderate x region, where the pionic Drell-Yan data are believed to be valid. In the moderate x regime, the Drell-Yan photon is predominantly transverse and nuclear corrections are minimal. Thus, we will measure the reaction p(e,e'n)X in the deep inelastic scattering regime which would correspond to an $x_\pi$ range of 0.4 to 0.8, and extract the pion structure function from the data.

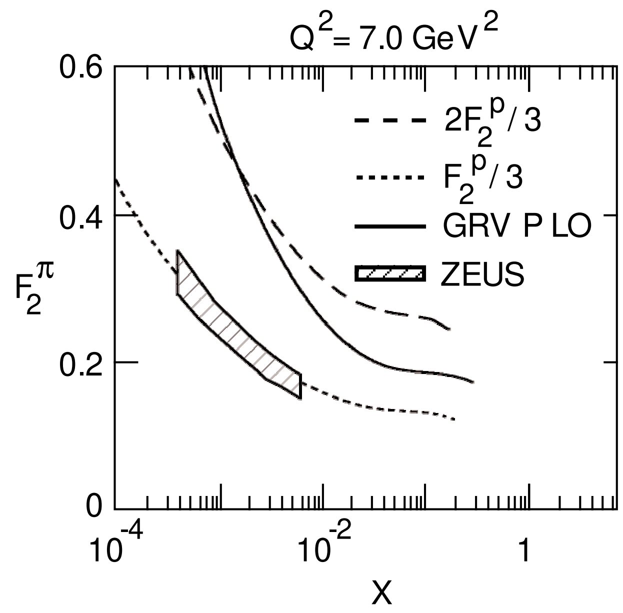


Figure 2: The pion structure function vs. x. The shaded band represents the ZEUS data. The dotted and dashed curves represent the proton structure function scaled by a factor of 1/3 and 2/3, respectively. The solid curve represents a leading order analysis which includes both the pionic Drell-Yan and prompt photon data[8]. From these data, it appears that the pion sea is only 1/3 of the proton sea.

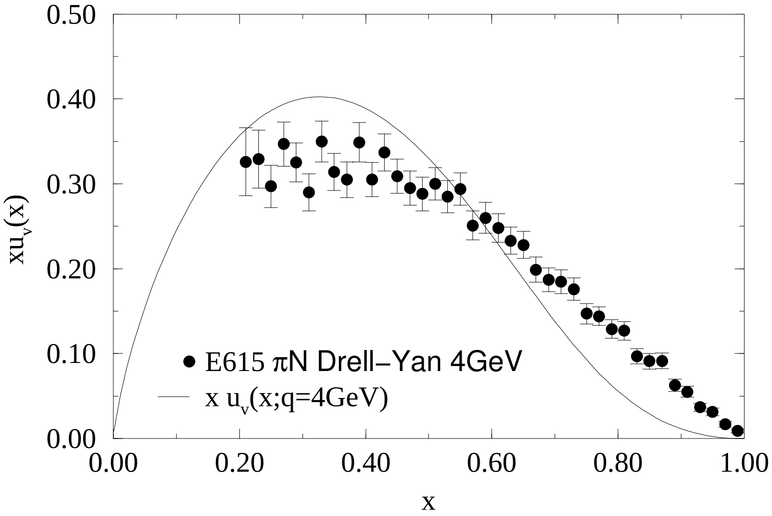


Figure 3: Existing data for the pion structure function from Drell-Yan scattering [7]. The solid curve represents a calculation of Hecht *et al.* [9], which is typical of treatments that describe the pion as a non pointlike bound state. There is a marked disagreement between the calculation and data at high x.

# 3 Proposed Measurements

The goal of the experiment is to provide data for the semi-inclusive reaction p(e,e'n)X for $Q^2 > 1GeV^2$ and as a function of the neutron momentum in the range 0.2 to 1.0 GeV/c. The experiment will focus on detection of low-energy neutrons. This means that the virtual pion also has a small three-momentum, and consequently, the pion cloud should be spatially large, where the validity of the pion cloud model should be enhanced.

We will be measuring the semi-inclusive structure function, $\mathrm{F}_2^{LN(4)}$, a model independent quantity, as given by the following equation:

The four fold differential cross-section for baryon production can be parameterized by a semi-inclusive structure function, $\mathrm{F}_2^{LN(4)}$ defined by,

$$\frac{d^4\sigma(ep \to eNX)}{dxdQ^2dzdt} = \frac{4\pi\alpha^2}{xQ^4}(1 - y + \frac{y^2}{2[1+R]})F_2^{LN(4)}(x, Q^2, z, t)$$

$$z = \frac{q \cdot p'}{q \cdot p}$$

$$t = (p - p\prime)^2$$

$$y = \frac{p \cdot q}{p \cdot k}$$

Where $\alpha$ is the fine structure constant, and R is the ratio between the absorption cross-sections for longitudinally and transversly polarized virtual photons, and p and p$'$ are the incident and out going baryon momenta. Since the structure function $F_2^{LN(4)}$ is rather insensitive to the value of R, for this analysis we will use R=0. If we now integrate over t by integrating over the neutron momentum from 200 MeV/c to 500 MeV/c, then we have

$$\frac{d^3\sigma(ep \rightarrow eNX)}{dxdQ^2dz} = \frac{4\pi\alpha^2}{xQ^4}(1 - y + \frac{y^2}{2})F_2^{LN(3)}(x, Q^2, z)$$

following the analysis of Adloff *et al*[5]. The statistical accuracy of the present experiment in the measurement of the leading neutron structure function $F_2^{LN(3)}(x, Q^2, z)$ is shown in Fig. 9.

Alternatly, we can also use a ratio measurement of coincidence to singles to measure the $F_2^L N(4)$(x,$Q^2$,z,t) as shown below:

$$\frac{d^4\sigma}{dxdQ^2dzdt} / \frac{d^2\sigma}{dxdQ^2}\Delta z \Delta t$$

then we have measured the ratio:

$$r = F_2^L N(4)(x, Q^2, z, t)/F_2(x, Q^2)^p$$

then

$$F_2^L N(4)(x, Q^2, z, t) = \frac{r}{\Delta z \Delta t} F_2^p(x, Q^2)$$

where $F_2^p$(x,$Q^2$) is the usual proton structure function that is known extremely well in this x and $Q^2$ range. This will greatly reduce systematic errors in luminosity, trigger effic., radiative corrections, etc.

# 4 Experiment

## 4.1 Overview

We are proposing to use JLAB 6 GeV unpolarized electron beam with a current of 2 $\mu$A. The target will be the standard Hall A 4 cm liquid hydrogen target. We will use the Hall A High Resolution Spectrometer Right (HRSR) and the Bigbite spectrometer to detect electrons in coincidence with neutrons detected in a plastic scintillator detector. The neutron detector will be placed behind the large opening of the Bigbite dipole, so that this dipole can be used as a sweeping magnet to remove charged particles. Detection of the scattered electron in two different spectrometers provides a systematic check of the electron scattering part of the experiment.

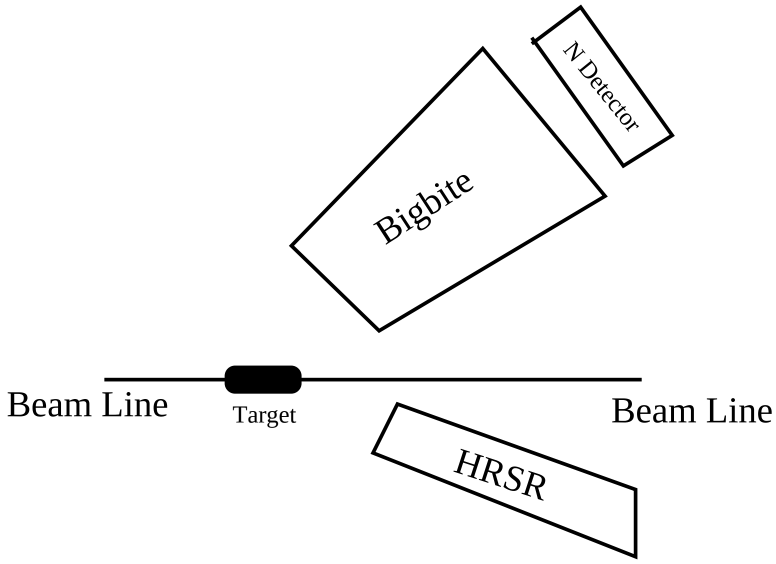


Figure 4: Experiment floor plan: HRSR and Bigbite spectrometer will be used to detect electrons; a plastic scintillator array behind the Bigbite spectrometer will be used to detect the neutrons in coincidence with the detected electrons in each spectrometer.

Approved Hall A experiment E01-015 (Studying the internal small-distance structure of nuclei via the triple coincidence (e,e′p+N) measurement) will use a simillar setup as proposed for this experiment. The neutron energy range for E01-015 is also very close to the present proposal.

## 4.2 The High Resolution Spectrometer Right (HRSR)

We will be using the HRSR to access the high $x_\pi$ region by going to a lower scattering angle of $25^0$. The central momentum will be about 2.0 GeV/c. The kinematics range accessed is shown in Fig.5. The coincidence neutrons will be detected by the neutron detector situated behind the Bigbite spectrometer. HRSR has a solid angle acceptance of about 6 msr and a momentum acceptance of ±4.5%. The maximum momentum is 3 GeV/c. We will be using it in the standard configuration with the standard detector package. HRSR has a $y_{tg}$ acceptance of ±5cm. Thus the 4 cm target will be fully visible in the high acceptance central region of $y_{tg}$.

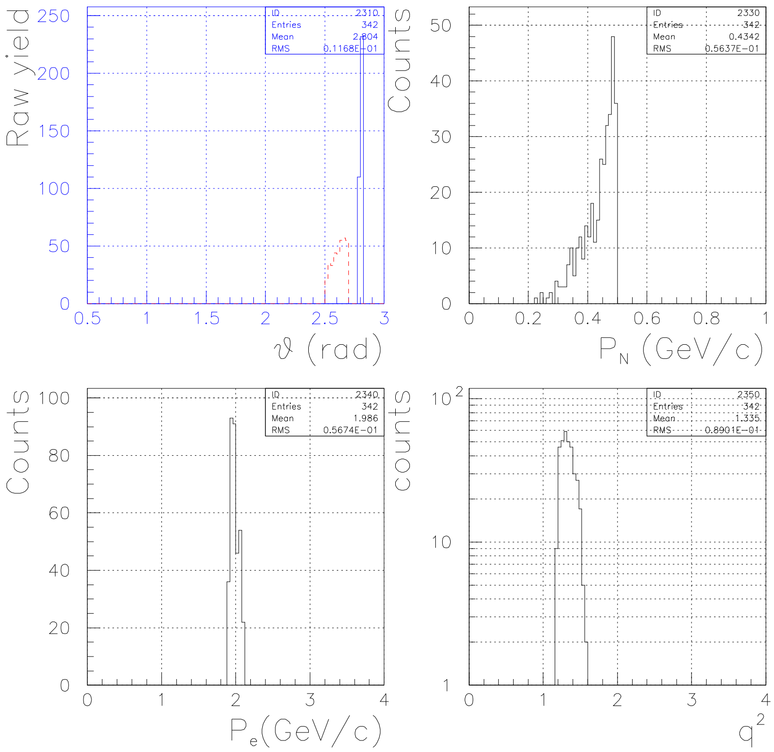


Figure 5: Simulated HRSE kinematics for the pion struture function experiment. Top left gives the central angle for HRSE and the neutron detector, top right gives the neutron momentum range accessed, bottom left gives the electron momentum range covered, and the bottom right gives the $q^2$ range covered.

Since we are accessing the Deep Inelastic Scattering (DIS) region, there will be a significant pion contamination. Thus good particle identification is necessary to separate electrons from $\pi^-$. For HRSR this is not a problem since it already has a gas $\hat{C}$erenkov detector and a lead-glass detector with a combined demonstrated $e^-/\pi^-$ rejection ratio of 1:10000. This will comfortably handle the expected $e^-/\pi^-$ background of 1/2.5 We will be incorporating the gas $\hat{C}$erenkov in the HRSR trigger setup to put a hardware cut on the pions so that we will not be data aquisition rate limited. This was already successfully used during the test run in April.

For a 2 $\mu$A beam with 4cm LH2 target, the real coincidence rates expected for the case of HRSR is 0.02 HZ and accidental coincidence rate in a 100 ns timing window is about 0.01 HZ. So the estimated signal to noise ratio is about 2:1. These singles rates for the neutron detector are expected to decrease when Bigbite is used to sweep away the charged particles.

## 4.3 The Bigbite Spectrometer

A significant amount of data for this experiment will be accessed using the Bigbite spectrometer in Hall A. The advantages of using Bigbite are four fold: It has a large momentum acceptance at low scattered electron momenta giving us access to the DIS region. Second, the large gap in the Bigbite dipole can accomodate the neutron detector behind the Bigbite spectrometer. This way the Bigbite spectrometer doubles as a sweeping magnet for the charged particles for the neutron detector, reducing the singles rates and cleaning up a significant amount of background. Third, it has a large solid angle. Fourth, the best kinematic coverage for this experiment is when both neutron detector and the electron spectrometer angles are simillar. This is achieved by placing the neutron detector behind the Bigbite spectrometer.

The Bigbite spectrometer was moved from NIKHEF to Hall A and is being refurbished now. It will be operated as a third arm in Hall A, and has large momentum and angular acceptances. At its maximum field setting, Bigbite can detect electrons with a momentum range of 250 to 900 MeV/c and a momentum resolution of $\Delta$p/p=0.8%. It has a solid angle coverage of 96 msr.

The Bigbite detector package is being rebuilt by the JLAB and the UVA groups. A group from Glasgow is already committed to providing new trigger scintillators for the Bigbite. This will consist of two layers of segmented plastic scintillators as shown in figure 7; one ($\Delta$E) with thin counters (3mm) and the second (E) with thick (3cm) counters, each segmented to 16 elements. This system is expected to give position independent mean time resolution of 0.5 ns FWHM and position information in the non-dispersive direction of 4 cm FWHM, and a momentum resolution of 10%.

As proposed by the approved experiment, E01-014, a set of multiwire

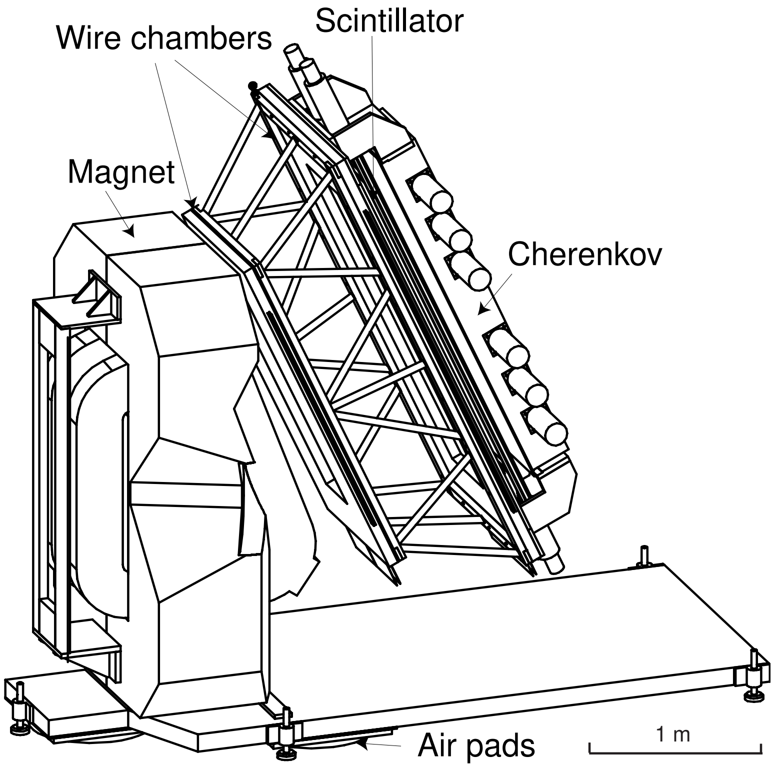


Figure 6: A schematic diagram of the Bigbite spectrometer showing the magnet and the detector system.

proportional chambers will be built for the Bigbite spectrometer in order to accomodate high luminosity. Since the experiment E01-014 is the comissioning experiment for Bigbite, it will also perform a careful study of the acceptance and optics required for the spectrometer.

Unlike the HRSE case, adequate particle ID detectors do not already exist for Bigbite. Bigbite has an aerogel $\hat{C}$erenkov detector which has mainly been used to separate p/$\pi^+$. By replacing the aerogel with a lower refractive index material, $e^-/\pi^-$ separation up to 1 GeV can be achieved. If this is not adequate, utilizing the available Pb glass blocks from the HRSL, a shower counter can be assembled for further $e^-/\pi^-$ separation. Such a device will be very useful for other DIS experiments that uses the Bigbite spectrometer (At 6 GeV with $30^0$ scattering angle for Bigbite, the expected $e^-/\pi^-$ ratio is about 1/2). As in the case of HRSR, we intend to incorporate pion rejection hardware in the trigger which will maintain the data rate at a reasonable

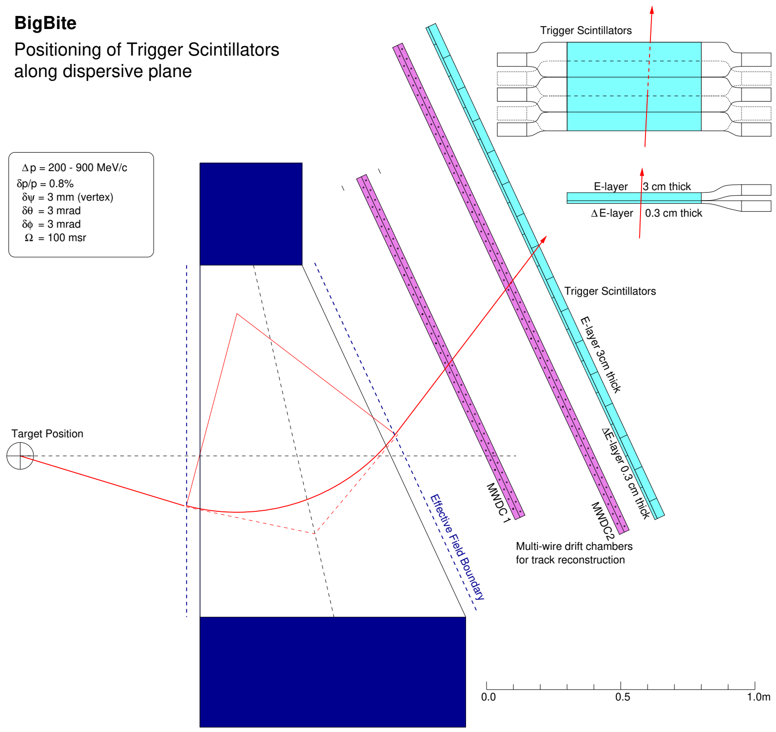


Figure 7: Schematic of the Bigbite spectrometer trigger scintillators

level.

We would position the Bigbite spectrometer at its minimum angle of $30^0$ from the beam line with the central momentum set to 0.7 GeV/c. The kinematic range accessed is shown in the figure 8. The coincidence neutrons will be detected by the previously mentioned neutron detector.

For 2 $\mu$A beam with 4cm LH2 target, the coincidence real rate expected for the case of Bigbite is 0.2 HZ while the coincidence background rate in a 100 ns timing window is about 0.16 HZ, giving a signal-to-noise ratio of about 1.25 to 1.

## 4.4 The Neutron Detector

We will detect neutrons in the momentum range of 200 to 1000 MeV/c. The pion cloud model is expected to be valid at low neutron momenta corresponding to a larger separation radius. For the analysis to isolate $F_2^{LN(3)}$ and $F_2^{\pi}$ we integrate only up to a neutron momentum of 500 MeV/c. Higher momentum

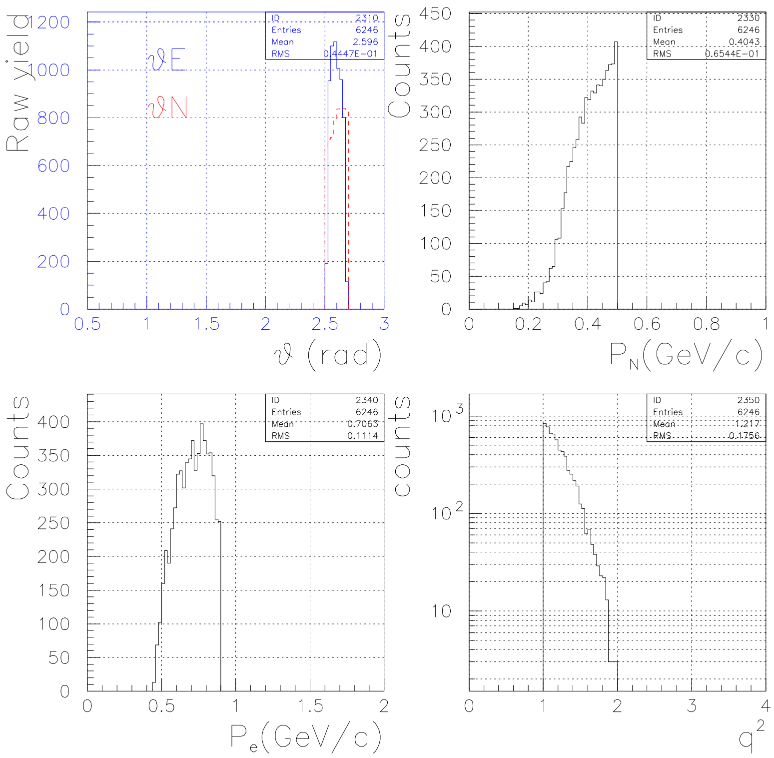


Figure 8: Simulated Bigbite kinematics for the pion structure function experiment. Top left gives the central angle for Bigbite and the neutron detector, top right gives the neutron momentum range of interest, bottom left gives the electron momentum range covered by Bigbite, and the bottom right gives the $q^2$ range covered.

data will allow us to check where the pion-cloud model loses it's validity.

For the neutron detector, we are proposing to use a similar setup as E01-015. The detector will be located behind Bigbite spectrometer, approximately 5 m from the target. It will consist of four walls with 6 plastic scintillators (160x10x10 $cm^3$) in each wall. In front of the neutron detector we will install a wall of veto detectors of thin scintillators (160x10x1 $cm^3$) to veto the remaining charged particles. The following rate and time estimates assume a 35% efficiency for the 40 cm thick neutron wall. We will also use a 1$''$ thick Pb wall in front of the neutron detector to filter out gamma rays and other low energy electromagnetic showers. A factor of 0.75 was assumed in the rate estimates for the neutron transmission efficiency through the Pb shielding.

### 4.4.1 Neutron Momentum Measurement.

The spread in coincidence time of flight between the slowest and the fastest neutrons for the proposed case will be about 50 ns. However we will use a wide concidence timing gate of about 300 ns. This will give a coincidence TOF spectrum with wide enough flat regions of accidental coincidence events in either side of the true coincidence bump in the middle. This method was checked during a test run in April. We will use the flat background regions to perform accidental background subtraction.

We are also interested in determining the momentum of neutrons in the 200 to 1000 MeV/c range (corresponding to 70 - 25 ns time of flight) using the TOF spectrum. First we will calibrate the TOF spectrum with known neutron momenta for the detected particles. For this we will use the p($\gamma$,$\pi^+$)n reaction. In this fully determined two-body reaction, neutron momentum can be calculated from the beam energy and the $\pi^+$ momentum. To adjust the neutron energy, we will move the HRSR to the forward angle to detect $\pi^+$ and the neutron counter to a large angle. By setting a very tight fiducial around the $\pi^+$ in the HRSR, we can make sure that all the neutrons produced by this reaction would strike the neutron counter, this will also enable us to measure the efficiency of the neutron counter at a given energy.

### 4.4.2 Missing mass resolution

It is expected that electron elastic scattering from the virtual pion cloud will contribute approximately 30% of the events. To separate the elastic scattering from the DIS scattering from the virtual pion, we will use the reconstructed missing mass. The missing mass resolution is limited by the momentum resolution of the detected neutrons and the angular resolution of the detected neutrons.

The momentum resolution of the detected neutrons is determined by our ability to measure the coincidence TOF. We expect to have a coincidence TOF resolution of 1 ns. This has already been achieved for the HRS pair. This will result a missing mass resolution of 65 MeV. The position information of the detected neutron along the scintillator bar is obtained by taking the difference of the TDC values from the PMTs at either end of the bar. This technique will give a position resolution of $\pm$ 5 cm ($\pm$10 mrad at 5 m from the target) which will result in a missing mass resolution of 30 MeV. Together these two will give a total missing mass resolution of 70 MeV, which is ample to separate the elastic scatering data from the DIS data. Due to much higher resolution available from the two electron spectrometers, uncertainties in $\vec{q}$ and $\nu$ have negligible contribution to the missing mass resolution.

### 4.4.3 Rates, Kinematics and Statistical Errors

Using the 6 GeV electron beam at JLAB with $Q^2 \geq 1$ in DIS scattering off the pion in the proton. For the rate calculations we have assumed a beam current of 2$\mu$A combined with a 4 cm LH2 target with a target density of about 1.686x$10^{23}$ atoms/cm$^2$ provides a luminosity of about 2.0x$10^{36}$ cm$^2$s$^{-1}$.

for a maximum statistical error of 10% measurement in the x and z bins, the time estimates are given below. In calculating the times we have assumed:

- Neutron detection efficiency of 35%.
- Neutron transmission factor of 0.75 in the Pb shielding.
- Beam current: 2 $\mu$A
- Target: 4 cm LH2
- Computer live time: 0.95
- Calibrating time for the neutron counters of 50 hours.
- Background rates for each bin is total background rate devided by the number of bins.

In conclusion we request total beam time of 12 days for the pion structure function experiment.

## 4.5 Systematic Errors

The systematic errors are divided into measurement errors of the p(e,e'n)X cross section as well as analysis and model errors in extracting the pion structure function for the discussion below. Overall systematic error in the measurement of the yield is estimated to be 8%. The largest contributions to this error are the spectrometer acceptance (3%), the neutron detector efficiency measurement (3%), radiative corrections ($< 4\%$), and the background

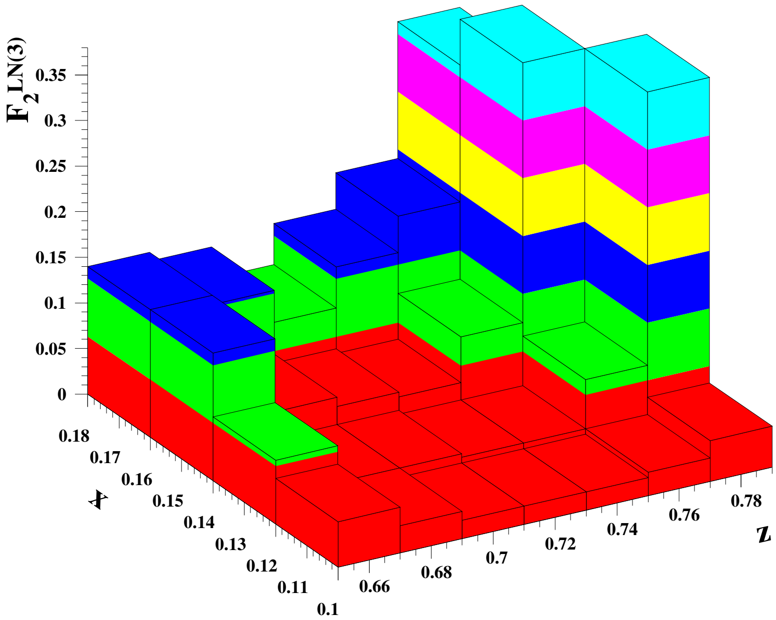


Figure 9: Simulated $x_{proton}$ and z range and the expected relative statistical error on $F_2^{LN(3)}(x, Q^2, z)$ as a function of $x_{proton}$ and z for the pion structure function experiment.

subtraction (5%). All other measurement errors, for example, in target thickness, beam current, particle identification, and electron detector efficiency are negligible by comparison.

# 5 Extraction of the Pion Structure Function

$F_2^{\pi}$ can be extracted from $F_2^{LN(3)}$ using some model assumptions. As an example of such an extraction, using the Regge model of baryon production, the contribution of a specific exchange i, is defined by the product of its particle flux $f_{i/p}$(z,t) and its structure function $F_2^i$ evaluated at ($x_\pi$,$Q^2$). For leading neutron production, with $p_T \leq$200 MeV.

$$F_2^{LN(3)}(x, Q^2, z) = \sum_i [\int_{t_0}^{t_{min}} f_{i/p}(z, t) dt] F_2^i(x_\pi, Q^2)$$

Where i denotes the pion, $\rho$-meson, etc. and the t corresponds to the range of $p_T$ analyzed. This is essentially the analysis performed for the

HERA data by the H1 Collaboration. Fig 10 shows the expected relative statistical errors on $x_\pi$ from this experiment.

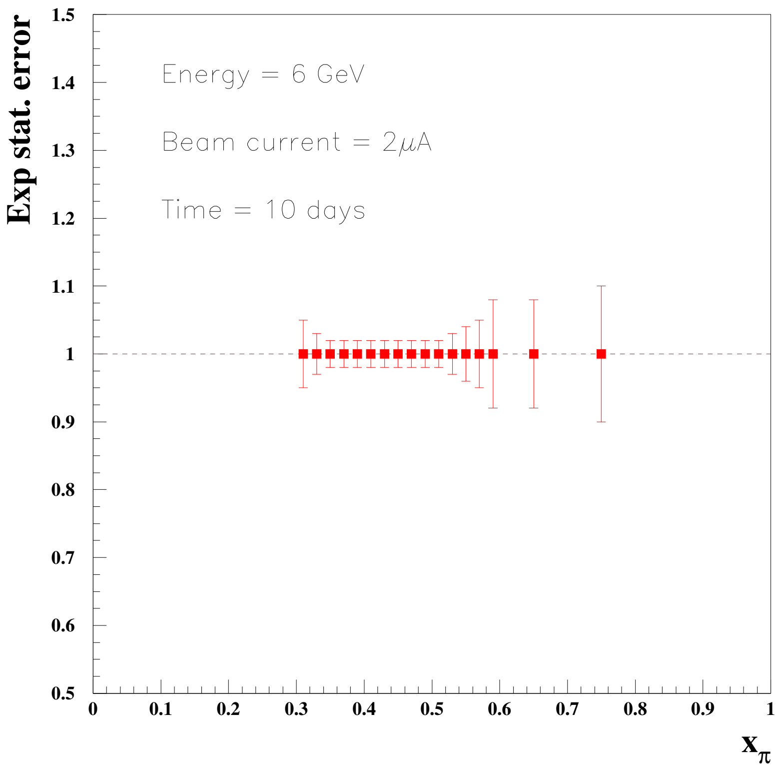


Figure 10: Simulated $x_\pi$ range and the expected relative statistical error for the pion structure function experiment.

Of course, the extraction of the pion structure function is not simple. There are absorptive effects as well as effects of other mesons, for example, the $\rho$ meson. These other corrections can be minimized by measuring the lowest neutron momenta possible from the reaction. This minimizes the absorptive correction since at lower momenta the pion cloud is further from the bare nucleon. In addition, the low neutron momenta ensure that the higher meson mass exchanges are suppressed by the energy denominator. These corrections have been treated in detail[18, 19] and are discussed below.

The largest uncertainty in extracting the pion structure function is the pion flux factor. A comparison of different flux factors as well as Reggeized flux factors has been discussed[19]. However, proposed work would follow a Regge calculation approach similar to that used for the pion form factor extraction[20, 21]. The pion structure function extracted from these analyses would then be compared with the structure function from pionic Drell-Yan measurements at moderate values of $x_\pi$.

## 5.1 Non-pion pole contribution

In the experiment, we aim to measure the p(e,e'n)X yield at the lowest values of t. This means that we are preferentially selecting the lowest mass meson, the pion. However, there could be some contamination from other light mesons, for example, the $\rho$ and $a_2$ mesons exchange or pion production. These processes would also lead to neutron production. Fortunately, the contamination from these processes has already been estimated to be negligible at low values of t[17].

## 5.2 $\Delta$ and higher $N^*$ production

The experiment will not have sufficient missing mass resolution to directly eliminate processes where a $\Delta$ is formed in the final state. This process has been estimated[18] to contribute approximately 15% to the pion flux. However, it turns out that the neutrons produced by this process are generally higher in energy than the neutrons that we will be selecting. Thus, the contribution from processes of this type are estimated to be less than 5%. The contibution from higher mass resonances would be much smaller than those from the $\Delta$. Thus, the uncertainty from this contribution to the pion flux would be less than 5%.

## 5.3 Absorptive Effects

Absorptive effects are expected to break the simple factorization scheme given by pure one pion exchange. Absorption arises because a photon has a finite transverse size governed by the momentum transfer, and thus, there is a probability of interacting with the bare nucleon as well as the pion cloud, even though one is near the Chew-Low limit. Absorptive corrections have been estimated by several authors[19, 22, 23]. The effect for the kinematics of this proposal is estimated to be approximately 15%.

### 5.4 Uncertainties in the pion flux

The largest uncertainty arises from a good understanding of the pion flux within the framework of the pion cloud model. One of the main issues is whether one uses merely a $\pi NN$ form factor or a Reggeized form factor. The difference between these two methods has been investigated[19] and can be as much as 20%. Perhaps this difference is responsible for the recent 12% correction[21] made to the pion form factors measured at DESY. The $\pi NN$ coupling constant is believed to be known to 5%. This uncertainty estimate is based on analyses[24] of N-N data.

If we assume that the corrections discussed above can be performed with a 50% uncertainty and we assume a 20% uncertainty in the pion flux factor, then the overall systematic uncertainty for measuring the pion structure function is approximately, 24%, where the largest uncertainty is in the pion flux determination. We note, however, that by comparing to pionic Drell-Yan data, we should have a calibration of this method at moderate values of x, where this data is most reliable and thereby provide a measurement of the pion flux factor. For example, the pion structure function at x=0.5 was measured[7] to an accuracy of 5%.

## 6 Acknowledgements

We are especially grateful for useful conversations with G. Levman, T.-S. H. Lee and F. Coester.

## References

[1] M. Alberg, E. M. Henley, G. A. Miller, *Phys. Lett.* **B471**, 396 (2000); N. N. Nikolaev *et al, Phys. Rev.* **D60**, 014004 (1999).

[2] Maris, P., Roberts, C.D., Tandy, P.C., *Phys. Lett.* **B420**, 287 (1998).

[3] A. W. Thomas, S. Theberge, G. A. Miller, *Phys. Rev.* **D24**, 216 (1981).

[4] J. Carlson and R. Schiavilla, *Rev. Mod. Phys.* **70**, 743 (1998).

[5] C. Adloff *et al. Eur. Phys. J.* **C 6**, 587 (1999); C.-P. Fagerstroem, Ph.D. Thesis, Univ. of Toronto (1999); G. Levman, Proc. of Workshop on Lepton Scattering, Hadrons and QCD, Univ. of Adelaide (2001).

[6] Suzuki, K., Weise, W. *Nucl. Phys.* **A634**, 141 (1998).

[7] Conway, J. S. *et al. Phys. Rev.* **D39**, 39 (1989).

[8] M Gluck, E Reya and A Vogt, Z. Phys. C53(1992)651.

[9] Hecht, M. B., Roberts, C. D., Schmidt, S. M., preprint (2000), nucl-th/0008049.

[10] Shigetani, T., Suzuki, K., Toki, H. *Phys. Lett.* **B308**, 383 (1993).

[11] Davidson, R. M., Arriola, E. Ruiz *Phys. Lett* **B348**, 163 (1995).

[12] Best, C. *et al. Phys. Rev.* **D56**, 2743 (1997).

[13] T. Frederico and G.A. Miller, Phys. Rev. **D 50**, 210 (1994)

[14] A.E. Dorokhov and L. Tomio, Phys. Rev. **D 62** 014016 (2000).

[15] S. J. Brodsky, M. Burkardt, I. Schmidt, *Nucl. Phys.* **B441**, 197 (1995); W. Melnitchouk, priv. comm. (2001).

[16] R. J. Holt and P. E. Reimer, Proc. of the Second Int'l Workshop on the Electron-Polarized Ion Collider, MIT, 2000.

[17] B. Kopeliovich and B. Povh, Z. Phys. C **73**, 125 (1996)

[18] H. Holtmann *et al.*, Phys. Lett. B **338**, 393 (1995)

[19] U. D'Alesio and H. J. Pirner *Eur. Phys. J* **A7**, 109 (2000).

[20] M. Vanderhaeghen, M. Guidal, J.-M. Laget Phys. Rev. C **57**, 1454 (1998); NPA **627**, 645 (1997).

[21] J. Volmer *et al* Phys. Rev. Lett. **86**, 1713 (2001).

[22] N. Nikolaev *et al* hep-ph/9708290.

[23] F. Carvalho *et al.*, Phys. Rev. D **60**, 094015 (2000)

[24] V. G. J. Stoks *Nucl. Phys.* **A629**, 205c (1998); V. G. J. Stoks and Th. A. Rijken, Phys. Rev. C **59**, 3009 (1999); V. Stoks *et al.*, Phys. Rev. C **47**, 512 (1993)